IEEE Access
Multidisciplinary | Rapid Review | Open Access Journal

SPECIAL SECTION ON EMERGING TECHNOLOGIES FOR DEVICE TO DEVICE COMMUNICATIONS

Received October 17, 2018, accepted November 5, 2018, date of publication November 15, 2018,
date of current version December 7, 2018.

Digital Object Identifier 10.1109/ACCESS.2018.2880988

Interference Mitigation Based on Optimal Modes Selection Strategy and CMA-MIMO Equalization for OAM-MIMO Communications

LEI WANG[1,2], (Member, IEEE), FA JIANG[1], MINGKAI CHEN[1], HAIE DOU[1,2], GUAN GUI[1], (Senior Member, IEEE), AND HIKMET SARI[1], (Fellow, IEEE)

[1]National Engineering Research Center for Communications and Network Technology, Nanjing University of Posts and Telecommunications, Nanjing 210003, China
[2]National Mobile Communications Research Laboratory, Southeast University, Nanjing 210018, China

Corresponding author: Guan Gui (guiguan@njupt.edu.cn)

This work was supported in part by the National Natural Science Foundation of China under Grants 61671253 and 61571240, in part by the Major Projects of the Natural Science Foundation of the Jiangsu Higher Education Institutions under Grant 16KJA510004, in part by the Open Research Fund of the National Engineering Research Center for Communication and Network Technology, Nanjing University of Posts and Telecommunications, under Grant TXKY17005, in part by the Open Research Fund of the National Mobile Communications Research Laboratory, Southeast University, under Grant 2016D01, in part by the Research Fund of the Nanjing University of Posts and Telecommunications under Grant NY218012, in part by the Postgraduate Research and Practice Innovation Program of Jiangsu Province under Grant KYCX18_0911, and in part by a project funded by the Priority Academic Program Development of Jiangsu Higher Education Institutions.

ABSTRACT Transmitting multiple independent data streams through the same medium can increase the capacity of line-of-sight-based wireless communication systems. One of the promising approaches is to utilize spatial multiplexing with multiple spatially separated transmission/reception pairs, for which inter-channel interference can be declined by employing multiple-input multiple-output (MIMO) signal processing at the receiving ends. The other approach is to use orbital angular momentum (OAM) multiplexing transmitting multiple data streams, which makes use of the orthogonality among OAM beams to reduce inter-channel interference and enable efficient demultiplexing. However, due to the practical limitations, the two methods are hard to maximize their advantages independently. In order to utilize the two merits, this paper proposes an OAM-MIMO communication scheme to employ the potential of both multiplexing methods. Based on the system, we implement the measurement of inter-channel interference and then utilize the optimal modes selection strategy and constant modulus algorithm MIMO equalization to further improve the system performance. Our work indicates that the combination of these two interference mitigation methods can guarantee the communication quality when pursuing high-speed communications. Simulation results are given to corroborate the proposed scheme.

INDEX TERMS Constant modulus algorithm (CMA), LOS communication, MIMO equalization, orbital angular momentum (OAM), optimal modes selection.

I. INTRODUCTION

To meet the explosive growth of wireless traffic demands, line-of-sight (LOS) based communication with fixed transceiver equipments gradually shows its huge potential advantage in many applications [1]–[4]. Multiplexing multiple data streams in a LOS communication system can significantly increase data capacity and spectrum efficiency [5]. An important approach is to utilize spatial multiplexing with multiple fixed transmission/reception antennas. Combined with multiple-input multiple-output (MIMO) signal processing, this can provide capacity gains compared with single antenna system [6], [7].

Recently, a set of orthogonal electromagnetic waves has become another potential approach to simultaneously transmit multiple data streams [8]–[10]. In such systems, multiple orthogonal waves are transmitted in the same coaxial direction and each electromagnetic wave carries an independent data stream. In the ideal case, the greater the number of multiplexed electromagnetic waves, the greater the channel capacity and spectral efficiency. Orbital angular

momentum (OAM), as an orthogonal characteristic of electromagnetic waves, has aroused great interest by researchers [11]–[15]. An electromagnetic wave with a helical transverse phase characterized by $\exp(-il\phi)$ carries an OAM related to l, where l is an unbounded integer and ϕ is the transverse azimuthal angle [16]. Moreover, OAM beams with different OAM modes are orthogonal to each other [17] for which a set of OAM beams with different modes can be multiplexed to transmit multiple data streams together along the direction of the same beam axis. According to [18], a spectral efficiency of 25.6 bit/s/Hz was implemented by polarization-multiplexed multiple OAM optical communication systems when modulating 16-quadrature-amplitude modulation signals over four OAM modes. The experiment in [19] realizes a 32 Gbit/s millimeter-wave data link using OAM multiplexing combined with polarization multiplexing over a single aperture pair.

Because of the orthogonality of OAM beams bringing to channel interference elimination and convenience for signal recovery, the researches arise great interest on OAM signal processing. Compared with MIMO system, OAM multiplexing system avoids the complicated MIMO-based signal processing, especially at high data rates [20], [21]. However, the propagation of OAM beam requires high quality. The misalignment of transceiver equipments [22] and the poor propagation environment may cause mode migration, i.e. falling into the superposition of multiple modes from a single mode, thus causing inter-channel interference. Besides, due to the spatial distribution of OAM beams, the larger the mode value l, the more scattered the intensity distribution [23], which makes it hard to detect high-order OAM modes. Therefore, the number of available OAM modes is usually limited to a certain set in practice, and the OAM beams with high-order mode are rarely used. So it is difficult to maximize the number of available channels by exploiting only one physical resource. There might exist the possibility of partially making use of the advantages of each multiplexing technique and utilizing both technologies to improve system performance [24]. The experimental results in [25] express that the capacity of a pure 4×4 MIMO system can be outperformed by a 2×2 OAM-MIMO system at a short link distance. Sreedevi and Rao [30] propose a new OAM spatial modulation millimeter wave communication system which can achieve significant performance gains over the conventional MIMO communication systems. Therefore, if each transceiver pair in spatial multiplexing systems multiplexes multiple different OAM beams, the total number of available channels will significantly increase and the spectrum efficiency will also improve.

Nevertheless, there is still some interference between channels when combining these two multiplexing approaches. If multiple OAM modes are multiplexed in the same link, the imperfect generation of OAM beam and the misalignment between transmitting and receiving device [27], [28] become the main sources of interference. While OAM multiplexing and spatial multiplexing are combined together, the source of inter-channel interference is significantly different from the pure OAM multiplexing system, which mainly comes from the other transmitters. Few researches have focused on this, and most of them can only confirm the existence of such interference through experiments [25], [29]. So it is necessary to measure the interference when combining these two multiplexing approaches. In this paper, we first construct an OAM-MIMO communication system, and then measure the inter-channel interference of this system.

In addition, the experiments in [25] show that MIMO-based signal processing can be used at the receivers of OAM-MIMO communication system to mitigate channel interference. Assuming that the interference distribution at receivers has been measured, the MIMO blind equalization algorithm can be utilized to enhance the bit error rate (BER) performance of the proposed OAM-MIMO communication system [31]. Moreover, OAM channel coding has become another potential way to eliminate inter-channel interference, such as low-density parity check (LDPC) precoded OAM modulation scheme [32] and Reed-Solomon (RS) coded interference mitigation scheme [33]. However, all these studies ignore the important property that the larger the difference between two modes, the smaller the possibility of mode migration between them [22] caused by inter-channel interference. By reasonably assigning the transmission modes in the OAM-MIMO system, the inter-channel interference can be eliminated to a certain extent at the transmitters. In this paper, we propose an optimal modes selection strategy, and prove that this strategy can be combined with MIMO blind equalization technology to further improve the performance of the OAM-MIMO communication system.

The remainder of this paper is outlined as follows. Section II describes the OAM-MIMO communication system. The measurement of inter-channel interference of this system is analyzed in Section III. Section IV introduces the inter-channel interference mitigation scheme based on optimal modes selection strategy and CMA-MIMO equalization. The simulation results are given in Section V. Conclusion is drawn in Section VI.

II. SYSTEM MODEL

The system model of LOS OAM-MIMO communications is illustrated in Fig. 1, where transmission/reception aperture pairs are arranged in a uniform linear structure for transmitting several OAM beams. And the distance between two adjacent transmitters or receivers is d, a constant in this communication system. Each of the transmission aperture $Tx_i(i = 1, 2, ...N)$ multiplexes M OAM beams with different OAM modes $(l_{i1}, l_{i2}, ..., l_{iM})$. At the receiving ends, N reception apertures $Rx_i(i = 1, 2, ...N)$ are utilized to capture the OAM beams from the N transmission apertures. Therefore, there is a number of NM data streams in this OAM-MIMO communication system.

The intensity of the OAM beam is mainly located in the ring region centered on the beam axis, and the radius of the ring increases with the increasing transmission

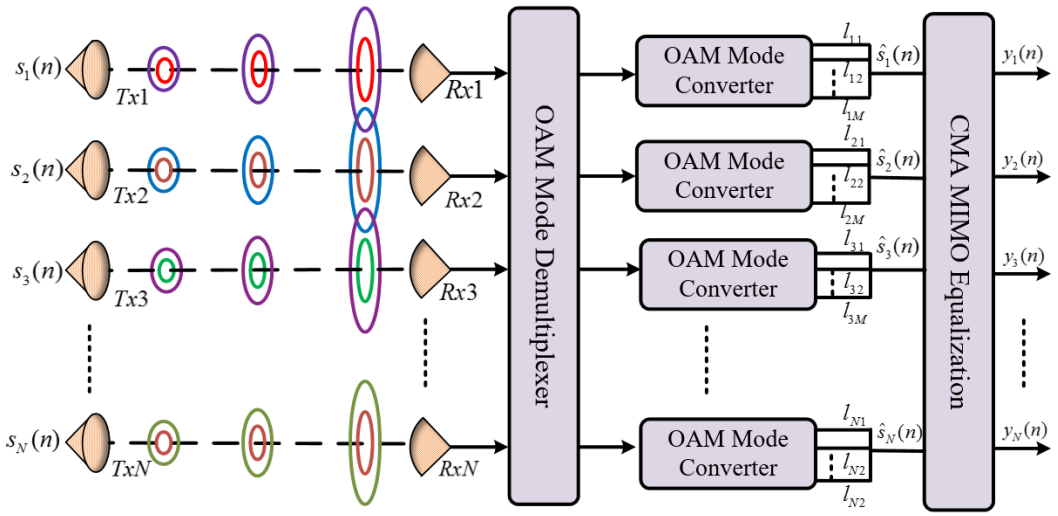

FIGURE 1. System model of OAM-MIMO communication system combined with CMA-MIMO equalization.

distance [17], [30]. Considering this spatial propagation characteristic of OAM beams, one receiver may receive OAM beams from the other transmitters. As previously described, transceiver pair Tx_i/Rx_i multiplexes M different OAM beams with mode $l_{im}(m = 1, 2, ..., M)$, which satisfies $l_{im} \neq l_{im'}(m, m' = 1, 2, ..., M)$. Besides, the mode values of the other transceiver pairs $Tx_j/Rx_j(j = 1, 2, ..., N; j \neq i)$ are $l_{jm}(m = 1, 2, ..., M)$ which satisfies $l_{im} \neq l_{jn}(m, n = 1, 2, ..., M)$. According to [15], when receiving the partial OAM beam of mode l_{jm} from transmitter $Tx_j(j \neq i)$, it can be seen equivalently as an incomplete reception due to the lateral displacement between Rx_i and Tx_j, which will induce the migration of mode l_{jm} and result in interference at the Rx_i. Based on this principle, the received signal vector of Rx_i can be expressed by

$$\hat{s}_i(n) = \sum_{j=1}^{N} h_{ij} s_j(n) + z_i, \tag{1}$$

where $\hat{s}_i(n) = (\hat{s}_{i1}(n), \hat{s}_{i2}(n), ..., \hat{s}_{iM}(n))^T$ and T represents the transpose operation of the matrix. $\hat{s}_{im}(n)(m = 1, 2, ..., M)$ denotes the received signal of mode l_{im} at the $i-th$ receiving aperture. $s_j(n) = (s_{j1}(n), ..., s_{jM}(n))^T$ is the transmission signal vector of Tx_j, and z_i represents the AWGN (Additional White Gaussian Noise) vector. Theoretically, the OAM beams of different mode values are orthogonal to each other, so the transmission matrix between Tx_i and Rx_i, i.e. h_{ii}, is a diagonal matrix. Moreover, due to the lateral displacement between Rx_i and Tx_j $(i \neq j)$, the non-diagonal elements of matrix $h_{ij}(i \neq j)$ are not zero. To sum up, the channel transfer matrix H can be expressed as

$$H = \begin{bmatrix} h_{11} & h_{12} & \cdots & h_{1N} \\ h_{21} & h_{22} & \cdots & h_{2N} \\ \vdots & \vdots & \cdots & \vdots \\ h_{N1} & h_{N2} & \cdots & h_{NN} \end{bmatrix}_{NM \times NM} \tag{2}$$

from which the inter-channel interference of the whole OAM-MIMO communications system caused by lateral displacement can be estimated. Based on (2), the transfer of the whole communications system can be written in the form of a matrix,

$$\hat{S}(n) = HS(n) + Z, \tag{3}$$

where $\hat{S}(n) = (\hat{s}_1(n), \hat{s}_2(n), ..., \hat{s}_N(n))^T$ and $S(n) = (s_1(n), s_2(n), ..., s_N(n))^T$. Z represents the AWGN column vector of $NM \times 1$. The CMA-MIMO equalizers are placed at the end of the entire communication system and utilized to correct the received signals in each data link.

III. INTER-CHANNEL INTERFERENCE MEASUREMENT

As mentioned in Section I, the interference between different OAM-MIMO channels mainly comes from the migration of OAM modes caused by the combined effects of tilt and lateral displacement equivalently. The interference of one receiver can be seen as the accumulation of interference from all the other transmitters. So we can establish a three-dimensional coordinate system with only two transceiver pairs to measure the inter-channel interference [22]. In Fig. 2, there are two transceiver pairs, Tx_1/Rx_1 and Tx_2/Rx_2. Tx_1/Rx_1 multiplexes mode l_2 along the Z-axis and Tx_2/Rx_2 multiplexes mode l_1 along the dashed line PR. Point $P(r_0, \theta_0)$ locates in $X - Y$ plane and dashed line $P - Q$ denotes the projection of $P - R$ on $X - Y$ plane. Besides, β is the angle between $P - Q$ and $P - P'$ which is parallel to X axis. When Rx_1 receives partial OAM beam from Tx_2, it will definitely cause interference because the incomplete receiving OAM beam of mode l_1 may partially migrate to mode l_2. So it is crucial to measure the inter-channel interference by scaling these two types of displacement. r_0 and θ_0 describe the lateral displacement, α and β describe the tilt displacement in Fig. 2.

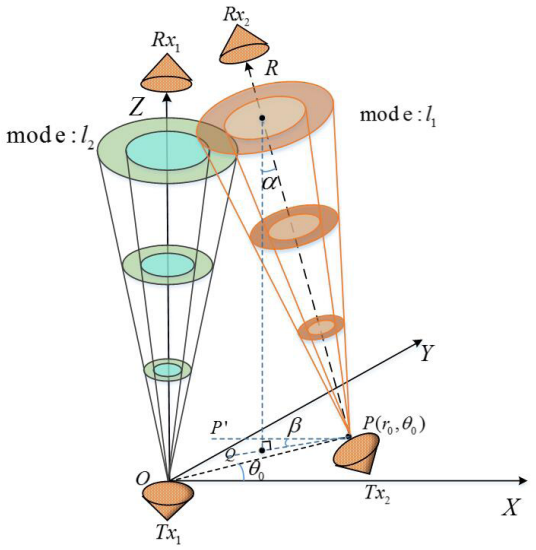

FIGURE 2. Inter-channel interference between two transceiver pairs caused by displacement.

An analytical expression which indicates the relation between inter-channel interference and displacement has been given as follows

$$C_{|l_1-l_2|}(u_0, v_0, \gamma) = \exp\left(-\frac{u_0^2+v_0^2}{4}\right)\left(\frac{\sqrt{u_0^4+v_0^4+2u_0^2v_0^2\cos(2\gamma)}}{u_0^2+v_0^2\pm 2u_0v_0\sin\gamma}\right) \times I_{|l_1-l_2|}\left(\frac{\sqrt{u_0^4+v_0^4+2u_0^2v_0^2\cos(2\gamma)}}{4}\right), \quad (4)$$

where $\gamma = \theta_0 - \beta$, $u_0 = 2r_0/w_0$. w_0 is the waist of the OAM beam and $k = 2\pi/\lambda$ is the wave number with λ being the wavelength. $I_{|l_1-l_2|}()$ is the $|l_1 - l_2|$th-order modified Bessel function of the first kind. Equation (4) represents the power percentage of the OAM beam with mode l_1 migrating to l_2 at Rx_1. When only one type of displacement exists, equation (4) can also be expressed as

$$C_{|l_1-l_2|} = \exp(-\zeta)\, I_{|l_1-l_2|}(\zeta), \quad (5)$$

where $\zeta = \frac{r_0^2}{w_0^2}$ for the lateral displacement-only case while $\zeta = \frac{k^2 w_0^2 (\sin\gamma)^2}{4}$ for the tilt displacement-only case.

Since all the transmission/reception pairs of the OAM-MIMO communication system are arranged in a two uniform parallel linear structure and the way of propagation is LOS, there is only the lateral displacement in our proposed communication system, i.e. $\zeta = \frac{r_0^2}{w_0^2}$. Equation (5) can be normalized for $\sum_{l_1-l_2=-\infty}^{\infty} \frac{C_{|l_1-l_2|}}{P} = 1$, where $P = \sum_{l_1-l_2=-\infty}^{\infty} \exp(-\zeta) I_{|l_1-l_2|}(\zeta)$. Thus, the corresponding power distribution of different modes after inter-channel interference happening can be determined when l_1 and the lateral displacement have been know. Here, the lateral displacement r_0 denotes the distance between two adjacent transmitting or receiving apertures in the proposed OAM-MIMO communication system, i.e. $d = r_0$.

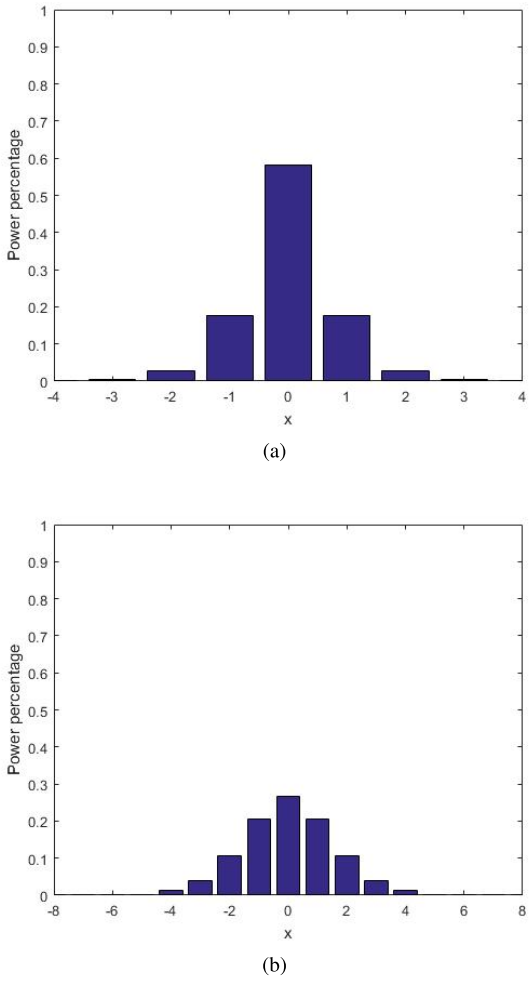

FIGURE 3. Power percentage of different OAM modes after mode migration with respect to $x = l_1 - l_2$.

As shown in Fig. 3, it is very clear that the power percentage decreases as the absolute value of x increases. Besides, Fig. 3 (a) and (b) represent the distribution of power percentage corresponding to $d/w_0 = 4/3$ and $d/w_0 = 8/3$. It indicates that the distance of adjacent transmitters d can also affect the distribution of power percentage after mode migration. When the transmission distance is fixed, mode migration will become more serious with the increasing d.

IV. INTER-CHANNEL INTERFERENCE MITIGATION SCHEME FOR THE OAM-MIMO COMMUNICATION SYSTEM

The proposed OAM-MIMO communication system is an ingenious combination of OAM multiplexing and spatial multiplexing. As mentioned before, although OAM beams of different modes are orthogonal to each other, the mode

migration caused by incomplete reception of OAM beams from the other transmitters will also induce inter-channel interference. In this section, we propose an interference mitigation scheme for the OAM-MIMO communication system which combines an optimal transmission modes selection strategy and CMA-MIMO blind equalization technology. And these two interference mitigation methods are presented in detail as follows.

A. OPTIMAL TRANSMISSION MODES SELECTION STRATEGY IN THE PROPOSED SCHEME

Equation (2) represents the channel transmission response matrix, where the non-diagonal elements are not zero due to mode migration at the receivers, thus becoming the main source of inter-channel interference except for the AWGN. To facilitate the elaboration of the optimal mode selection strategy, we let $N = M = 2$, i.e there are two transmission/reception pairs (Tx_1/Rx_1, Tx_2/Rx_2) and each pair multiplexing two OAM beams (l_{11}, l_{12} and l_{21}, l_{22}). Under this premise, the channel transfer matrix of the system can be written as

$$H_{4\times4} = \begin{bmatrix} h_{11,11} & h_{11,12} & h_{11,21} & h_{11,22} \\ h_{12,11} & h_{12,12} & h_{12,21} & h_{12,22} \\ h_{21,11} & h_{21,12} & h_{21,21} & h_{21,22} \\ h_{22,11} & h_{22,12} & h_{22,21} & h_{22,22} \end{bmatrix}_{4\times4}, \quad (6)$$

where

$$h_{im,jn} = \begin{cases} B\dfrac{\lambda}{4\pi d_{TR}} e^{-ikd_{TR}} & i = j, m = n \\ 0 & i = j, m \neq n \\ B\dfrac{\lambda}{4\pi d_{ij} P_{im,jn}} e^{-ikd_{ij}} C_{|l_{im}-l_{jn}|} & i \neq j \ or \ m \neq n \end{cases} \quad (7)$$

and $i, j, m, n \in \{1, 2\}$. B represents the gain of the transmitting antenna, d_{TR} represents the distance between Tx_1 and Rx_1. λ is the wavelength and $k = 2\pi/\lambda$ is the wave number. $d_{ij} = \sqrt{d_{TR}^2 + (i-j)^2 d^2}$ and d is the distance of adjacent transmitters or receivers. In addition, $P_{im,jn} = \sum_{\Delta l=-\infty}^{\infty} \exp(-\frac{(i-j)^2 d^2}{w_0^2}) I_{|\Delta l|}(\frac{(i-j)^2 d^2}{w_0^2})$, $C_{|l_{im}-l_{jn}|} = \exp\left(-\frac{(i-j)^2 d^2}{w_0^2}\right) I_{|l_{im}-l_{jn}|}(\frac{(i-j)^2 d^2}{w_0^2})$, where w_0 denotes the waist of the OAM beam. By substituting (7) into (6), equation (6) can be reduced to

$$H_{4\times4} = \frac{B\lambda e^{-ikd_0}}{4\pi d_0} \begin{bmatrix} A & 0 & \frac{C_{|l_{11}-l_{21}|}}{P_0} & \frac{C_{|l_{11}-l_{22}|}}{P_0} \\ 0 & A & \frac{C_{|l_{12}-l_{21}|}}{P_0} & \frac{C_{|l_{12}-l_{22}|}}{P_0} \\ \frac{C_{|l_{21}-l_{11}|}}{P_0} & \frac{C_{|l_{21}-l_{12}|}}{P_0} & A & 0 \\ \frac{C_{|l_{22}-l_{11}|}}{P_0} & \frac{C_{|l_{22}-l_{12}|}}{P_0} & 0 & A \end{bmatrix}_{4\times4}, \quad (8)$$

where A is a constant which satisfies $A = \frac{e^{-ik(d_{TR}-d_0)}d_0}{d_{TR}}$. $d_0 = \sqrt{d_{TR}^2 + d^2}$, and

$$P_{im,jn} = P_0 = \sum_{\Delta l=-\infty}^{\infty} \exp(-\frac{d^2}{w_0^2}) I_{|\Delta l|}(\frac{d^2}{w_0^2}). \quad (9)$$

Due to the rapid power decay and spatial distribution characteristic of OAM beams, we assume that the maximum OAM mode to be selected is L. It's worth noting that the non-diagonal elements of $H_{4\times4}$ should be as small as possible to make the BER of receivers as small as possible, and the value of non-diagonal elements in the matrix is directly related to the modes selection of transmitters. Moreover, $H_{4\times4}$ is a diagonal matrix, so the optimal mode selection strategy is to make the non-diagonal elements in the upper right-hand of $H_{4\times4}$ as small as possible. As depicted in Fig. 3, the greater the difference between two OAM modes, the lower the probability of mode migration between them due to lateral displacement. In short, the value of $\frac{C_{|l_{im}-l_{jn}|}}{P_{im,jn}}$ is inversely proportional to $|l_{im} - l_{jn}|$.

Suppose the set of available modes is $\Gamma = \{1, 2, ..., L-1, L\}$, where L satisfies $L \geq 4$. The optimal mode selection strategy is to select the first and last two modes of Γ, i.e., transceiver pair Tx_1/Rx_1 utilizes mode 1 and 2 while Tx_2/Rx_2 utilizes mode $L-1$ and L. For the case where $N, M > 2$, we first divide the ordered set of available modes into N mode subsets, then select the smallest M modes from the first subset and the largest M modes from the last subset. Finally, the M modes with middle size are selected from the other subsets. For example, when $N = M = 3$ and $\Gamma = \{1, 2, ..., 14, 15\}$, Γ can be equally divided into 3 mode subsets $\{1, 2, 3, 4, 5\}$, $\{6, 7, 8, 9, 10\}$ and $\{11, 12, 13, 14, 15\}$. For these three transceiver pairs, the corresponding OAM beams in $\{1, 2, 3\}$, $\{7, 8, 9\}$ and $\{13, 14, 15\}$ are utilized for data transmission.

B. CMA-MIMO BLIND EQUALIZATION IN THE PROPOSED SCHEME

Since the inter-channel interference at the receivers has been measured in Section III, MIMO blind equalization can be utilized to mitigate the inter-channel interference to improve the performance of each channel. CMA-MIMO equalization as a blind equalization technology has characteristics of low computational complexity and fast convergence speed, which meets the requirement of high rate transmission of the proposed communication system.

The principle of CMA-MIMO equalization is shown in Fig. 4. Each input signal vector of this module is denoted by $\hat{s}_i(n) = (\hat{s}_{i1}(n), \hat{s}_{i2}(n), ..., \hat{s}_{iM}(n))^T (i = 1, 2, ...N)$, which also represents the output signal vector of OAM mode converters. CMA-MIMO adaptive equalization utilizes a linear equalizer for each channel. In the proposed OAM-MIMO communication system, there are a number of NM data streams, so the whole equalization module includes $NM \times NM$ adaptive finite-impulse-response (FIR) filters with a tap number of K.

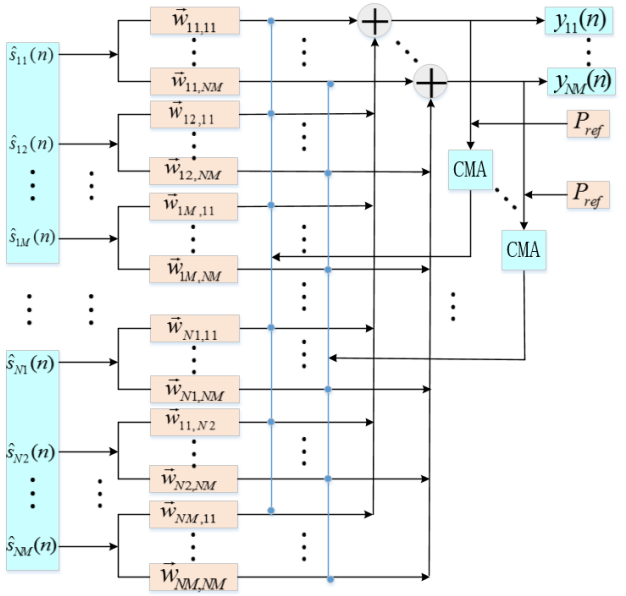

FIGURE 4. CMA-MIMO equalization.

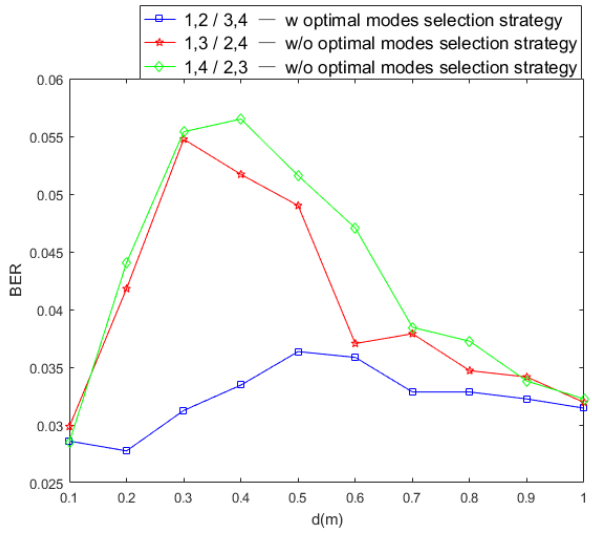

FIGURE 5. BER performance of channel I_{11} under different lateral displacements with and without optimal mode selection strategy.

It is an obvious truth that the FIR filters can help reduce the inter-channel interference. The output signal vector of Rx_i can be denoted by $y_i(n) = (y_{i1}(n), y_{i2}(n), ..., y_{iM}(n))^T$, $y_{im}(n)(m = 1, 2, ..., M)$ can be expressed as

$$y_{im}(n) = \sum_{j=1}^{N} \sum_{c=1}^{M} \sum_{k=0}^{K-1} w_{jc,im}^{k}(n) \hat{s}_{jc}(n-k), \tag{10}$$

where $w_{jc,im}^{k}(n)(i = 1, 2, ...N, m = 1, 2, ..., M)$ is the k-th tap coefficient of each FIR filter. $\hat{s}_{jc}(n-k)$ represents the receiving signal carried by the OAM beam with mode l_{jc} $(j = 1, 2, ...N; c = 1, 2, ..., M)$ from Tx_j at the $(n-k)$-th moment. Only $w_{jc,im}^{0}(n)$ are initialized as 1 and the other coefficients are initialized as 0. Then, all the coefficients are updated until the coefficients converge based on CMA,

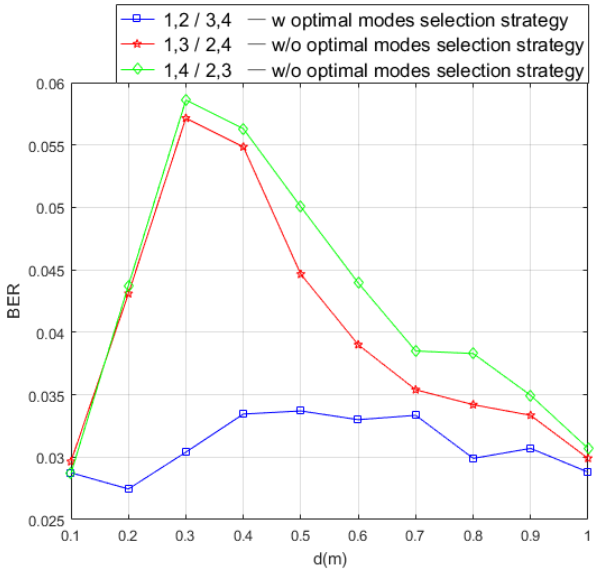

FIGURE 6. BER performance of channel I_{22} under different lateral displacements with and without optimal mode selection strategy.

the updating rules can be expressed as

$$\vec{W}_{jc,im}(n+1) = \vec{W}_{jc,im}(n) + u \cdot e_{im}(n) \cdot y_{im}(n) \cdot \vec{\hat{s}}_{jc}(n), \tag{11}$$

where $\vec{W}_{jc,im}(n) = [w_{jc,im}^{0}(n), w_{jc,im}^{1}(n), ..., w_{jc,im}^{K-1}(n)]^T$ denotes the tap coefficient vector of the equalizer at the n-th moment, K and T represents the vector length (tap number) and the transpose operation respectively. u is the step size of the updating process. The error signal of the adaptive equalization can be expressed as

$$e_{im}(n) = P_{ref} - |y_{im}(n)|^2, \tag{12}$$

where P_{ref} represents the normalized reference power and $||$ denotes the modular operation. $\vec{\hat{s}}_{jc}(n) = [\hat{s}_{jc}(n), \hat{s}_{jc}(n-1), \ldots, \hat{s}_{jc}(n-K+1)]^T$ is the input signal vector of the updated process. After a period of time, the weight vectors of the NM FIR filters reach convergence state, and the output of each FIR filter can be regarded as the optimal recovery signal under CMA criterion, thus achieving the purpose of reduce inter-channel interference.

It is obvious to see that the key to implement updating process is to work out $\hat{s}_{jc}(n)$ based on the measurement of interference. Suppose that the distance between Tx_i and Rx_i is d_{TR} and the distance of adjacent transmitters or receivers is d. Thus the distance from Tx_i to Rx_i can be obtained by $d_{ij} = \sqrt{d_{TR}^2 + (i-j)^2 d^2}$ $(i.j = 1, 2, ..., N)$. According to the interference measurement in Section III, $\hat{s}_{jc}(n)$ can be expressed as

$$\begin{aligned}\hat{s}_{jc}(n) &= \sqrt{p} \sum_{q=1, q\neq j}^{N} \sum_{m=1}^{M} h_{qm,jc} s_{qm}(n) + \sqrt{p} h_{jc,jc} s_{jc}(n) + z_{jc} \\ &= \sqrt{p} \sum_{q=1, q\neq j}^{N} \sum_{m=1}^{M} B \frac{\lambda}{4\pi d_{qj} P_{qm}} e^{-ikd_{qj}} C_{|l_{qm}-l_{jc}|} s_{qm}(n) \\ &\quad + \sqrt{p} B \frac{\lambda}{4\pi d_{TR}} e^{-ikd_{TR}} s_{jc}(n) + z_{jc},\end{aligned} \tag{13}$$

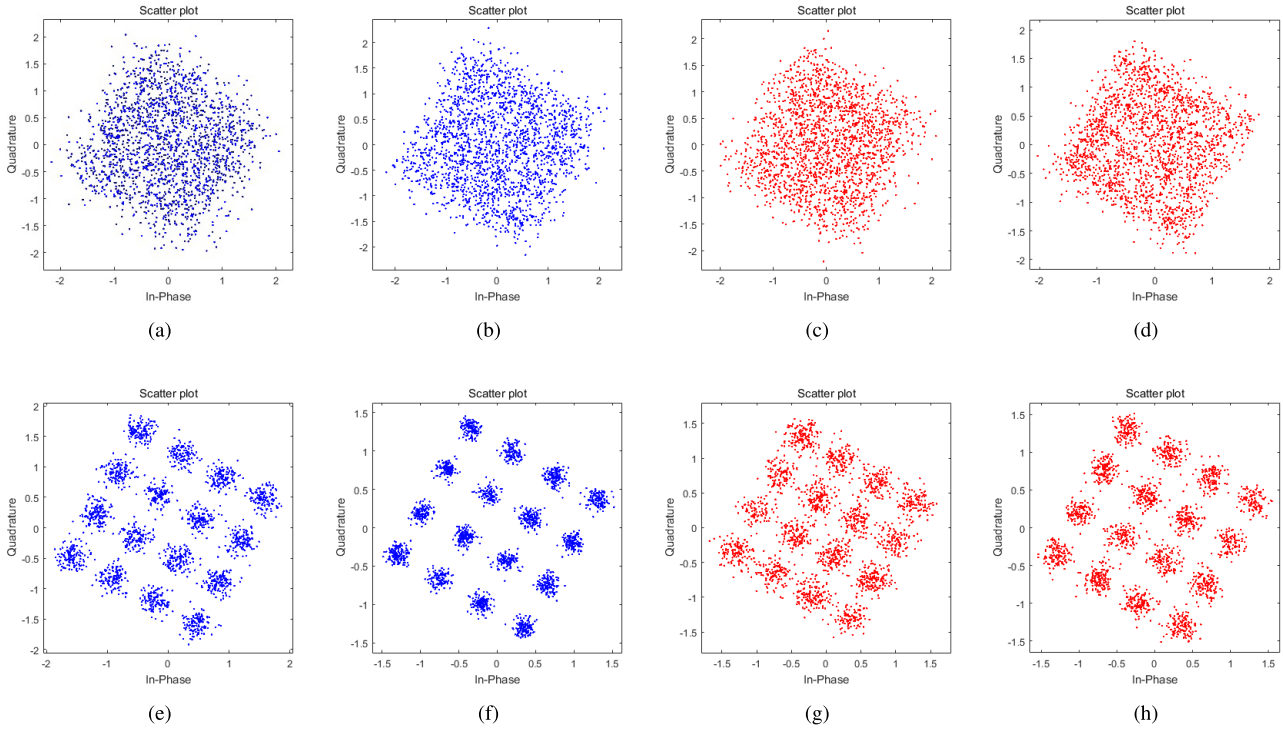

FIGURE 7. The 16 QAM signal constellation aberration caused by OAM mode migration due to incomplete reception of OAM beams from the other transmitter with and without CMA-MIMO equalization.(a)-(d)without CMA-MIMO equalization, (e)-(h) with CMA-MIMO equalization.

where p represents the transmission power of the OAM-MIMO communication system and $P_{qm} = \sum_{l_{qm}-l=-\infty}^{\infty} \exp(-\zeta) I_{|l_{qm}-l|}(\zeta)$. $h_{qm,jc}$ is the channel response between the m-th data link of Tx_i and the c-th data link of Rx_j. B represents the gain of the transmitting antenna. λ is the wavelength and $k = 2\pi/\lambda$ is the wave number.

V. NUMERICAL SIMULATION RESULTS

In this section, to make the proposed interference mitigation scheme more clear, we let $N = M = 2$, i.e. the OAM-MIMO communication system consists of two transmission/reception pairs and each pair multiplexes two different OAM beams. Specially, two transmission/reception pairs correspond to Tx_1/Rx_1 and Tx_2/Rx_2. Tx_1/Rx_1 and Tx_2/Rx_2 multiplex OAM beams from set $\Gamma = \{1, 2, 3, 4\}$. Therefore, there is a number of $NM = 4$ data links in this communication system corresponding to channel l_{11}, l_{12} in Tx_1/Rx_1 and channel l_{21}, l_{22} in Tx_2/Rx_2. Each of the four OAM channels carries a 16 QAM signal.

A. INTER-CHANNEL INTERFERENCE MITIGATION EFFECT BY OPTIMAL MODE SELECTION STRATEGY

In order to verify the advantages of our proposed mode selection strategy, we consider a more extreme situation, that is, only four modes 1, 2, 3, 4 are available for selection. By comparing the BER of Rx_1/Rx_2 along with different mode selection schemes, the performance of different schemes can be compared very well. Considering the symmetry of transceiver pair Tx_1/Rx_1 and Tx_2/Rx_2, there are three mode selection schemes from the point of pure mathematics. They are $\{1, 2\}\{3, 4\}$, $\{1, 3\}\{2, 4\}$ and $\{1, 4\}\{2, 3\}$.

As shown in Fig. 5 and Fig. 6, the horizontal axis represents the lateral interval between Rx_1 and Rx_2, and the vertical axis represents the BER at channel l_{11} and l_{22} respectively when the signal-to-noise ratio (SNR) is 5dB. It's clear that the BER performance of our proposed optimal mode selection scheme, i.e. $\{1, 2\}\{3, 4\}$, is better than the other two schemes. Besides, the BER performance difference of these three schemes is not very large when d tends to 1. Thus the advantages of the optimal mode selection scheme is not very obvious in the case of larger d.

B. INTER-CHANNEL INTERFERENCE MITIGATION EFFECT BY CMA-MIMO EQUALIZATION

Fig. 7 shows the 16 QAM signal constellation aberration caused by OAM mode migration due to incomplete reception of OAM beams from the other transmitters. For the first channel of Tx_1/Rx_1 corresponding to $l_{11} = +1$, Fig. 7 (a) and (b) represent the aberrated 16 QAM signal without CMA-MIMO equalization when the distance of adjacent transmitters or receivers satisfies $d = 0.8m$ and $d = 0.4m$ respectively. Fig.7 (e) and (f) represent the constellation diagram after the CMA-MIMO equalization processing. Similarly, Fig. 7 (c)-(d) and (g)-(h) denote the constellation diagram before and after equalization corresponding to channel $l_{22} = +4$. The comparison between constellation

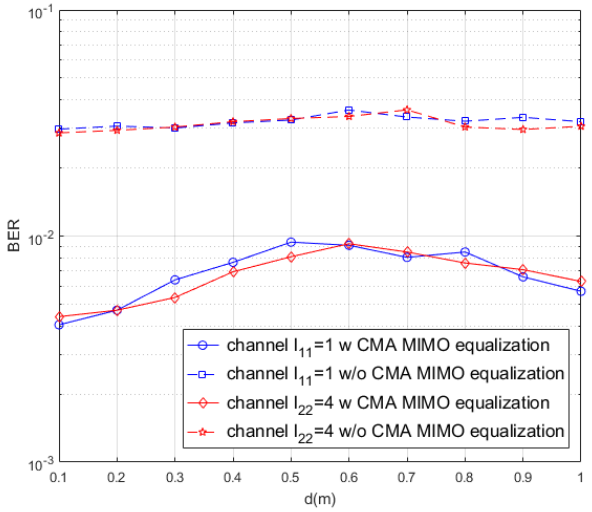

FIGURE 8. BER performance of channel $l_{11} = +1$ and $l_{22} = +4$ under different lateral displacements with and without CMA-MIMO equalization.

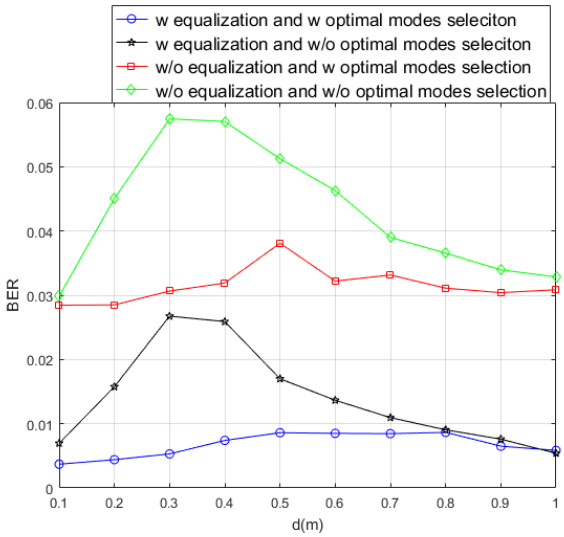

FIGURE 9. BER performance of channel l_{11} under different lateral displacements with both optimal modes selection and CMA-MIMO equalization.

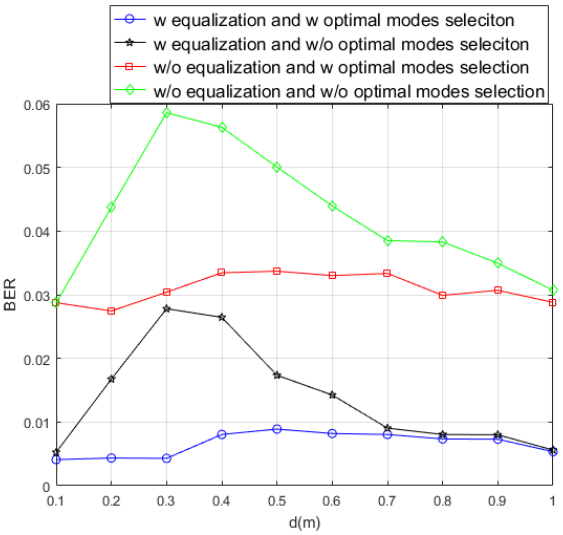

FIGURE 10. BER performance of channel l_{22} under different lateral displacements with both optimal modes selection and CMA-MIMO equalization.

diagrams shows that CMA-MIMO equalization technology can effectively improve the performance of OAM-MIMO communication system.

Fig. 8 shows the BER performance of channel $l_{11} = +1$ and $l_{22} = +4$ with and without CMA-MIMO equalization mitigation scheme against d. Here the distance of adjacent receivers d varying from $0.1m$ to $1m$ represents the lateral displacement extent from weak to strong. It is observed that two colors representing two OAM modes $l_{11} = +1$ and $l_{22} = +4$. The solid lines shows the BER performance with CMA-MIMO equalization, while the dotted lines without CMA-MIMO equalization. The results show that the BER performance of channel $l_{11} = +1$ and $l_{22} = +4$ with CMA-MIMO equalization is much better than without CMA-MIMO equalization.

C. INTER-CHANNEL INTERFERENCE MITIGATION EFFECT BY BOTH OPTIMAL MODE SELECTION STRATEGY AND CMA-MIMO EQUALIZATION

Finally, we demonstrate the inter-channel interference mitigation effect by utilizing both optimal mode selection strategy and CMA-MIMO equalization. Fig. 9 and Fig. 10 show the BER performance of channel l_{11} and l_{22} with both optimal modes selection and CMA-MIMO equalization. Here, optimal mode selection strategy corresponds to $l_{11} = +1$, $l_{12} = +2$, $l_{21} = +3$ and $l_{22} = +4$. The results show that the BER performance of OAM-MIMO communication links has been greatly improved by using both optimal modes selection strategy and CMA-MIMO equalization. The BER performance is better than those results utilizing optimal modes selection or CMA-MIMO equalization individually. We can draw that compared with the state-of-the-art equalization only approaches our proposed scheme performs better to eliminate the inter-channel interference of OAM-MIMO communication.

VI. CONCLUSION

In this paper, we have estimated the inter-channel interference caused by the mode migration for the partial reception of OAM beams from the other transmitters. Moreover, we proposed an inter-channel interference mitigation scheme based on optimal modes selection strategy and CMA-MIMO equalization for OAM-MIMO communication system. The numerical results has confirmed our point that applying the combination of these two methods to OAM-MIMO communication system can significantly reduce the inter-channel interference and improve the system performance. In the future work, we will further evaluate the advantages and disadvantages of this scheme in different cases.

REFERENCES

[1] S. Koenig *et al.*, "Wireless sub-THz communication system with high data rate," *Nature Photon.*, vol. 7, no. 12, pp. 977–981, Dec. 2013.
[2] Y. Li, Z. Zhang, H. Wang, and Q. Yang, "SERS: Social-aware energy-efficient relay selection in D2D communications," *IEEE Trans. Veh. Technol.*, vol. 67, no. 6, pp. 5331–5345, Jun. 2018, doi: 10.1109/TVT.2018.2810162.
[3] G. Gui, H. Huang, Y. Song, and H. Sari, "Deep learning for an effective nonorthogonal multiple access scheme," *IEEE Trans. Veh. Technol.*, vol. 67, no. 9, pp. 8440–8450, Sep. 2018.
[4] H. Huang, J. Yang, H. Huang, Y. Song, and G. Gui, "Deep learning for super-resolution channel estimation and DOA estimation based massive MIMO system," *IEEE Trans. Veh. Technol.*, vol. 67, no. 9, pp. 8549–8560, Sep. 2018.
[5] H. Zhang, R. Wang, H. Wang, and G. Wu, "A new lossless fault-tolerance mechanism in hybrid wireless-optical broadband access network," *IEEE Access*, vol. 6, pp. 19427–19440, 2018.
[6] L. Zhou, D. Wu, Z. Dong, and X. Li, "When collaboration hugs intelligence: Content delivery over ultra-dense networks," *IEEE Commun. Mag.*, vol. 55, no. 12, pp. 91–95, Dec. 2017.
[7] H. Chen, Z. Wang, F. Xia, Y. Li, and L. Shi, "Efficiently and completely identifying missing key tags for anonymous RFID systems," *IEEE Internet Things J.*, vol. 5, no. 4, pp. 2915–2926, Aug. 2018.
[8] G. Gibson, J. Courtial, M. J. Padgett, M. Vasnetsov, and V. Pas'ko, "Free-space information transfer using light beams carrying orbital angular momentum," *Opt. Exp.*, vol. 12, no. 22, pp. 5448–5456, 2004.
[9] D. Wu, F. Zhang, H. Wang, and R. Wang, "Fundamental relationship between node dynamic and content cooperative transmission in mobile multimedia communications," *Comput. Commun.*, vol. 120, pp. 71–79, May 2018.
[10] H. Chen, G. Ma, Z. Wang, Q. Wang, and J. Yu, "MAC: Missing tag iceberg queries for multi-category RFID systems," *IEEE Trans. Veh. Technol.*, to be published, doi: 10.1109/TVT.2018.2863726.
[11] J. Wang *et al.*, "Terabit free-space data transmission employing orbital angular momentum multiplexing," *Nature Photon.*, vol. 6, pp. 488–496, Jun. 2012.
[12] L. Zhou, D. Wu, J. Chen, and Z. Dong, "Greening the smart cities: Energy-efficient massive content delivery via D2D communications," *IEEE Trans. Ind. Informat.*, vol. 14, no. 4, pp. 1626–1634, Apr. 2018.
[13] L. Zhou, D. Wu, J. Chen, and Z. Dong, "When computation hugs intelligence: Content-aware data processing for industrial IoT," *IEEE Internet Things J.*, vol. 5, no. 3, pp. 1657–1666, Jun. 2018.
[14] I. B. Djordjevic, "Multidimensional OAM-based secure high-speed wireless communications," *IEEE Access*, vol. 5, pp. 16416–16428, 2017.
[15] R. Chen, W. Yang, H. Xu, and J. Li, "A 2-D FFT-based transceiver architecture for OAM-OFDM systems with UCA antennas," *IEEE Trans. Veh. Technol.*, vol. 67, no. 6, pp. 5481–5485, Jun. 2018.
[16] L. Allen, M. Beijersbergen, R. J. C. Spreeuw, and J. P. Woerdman, "Orbital angular momentum of light and the transformation of Laguerre-Gaussian laser modes," *Phys. Rev. A, Gen. Phys.*, vol. 45, no. 11, pp. 8185–8189, Jun. 1992.
[17] L. Wang, F. Jiang, Z. Yuan, J. Yang, G. Gui, H. Sari, "Mode division multiple access: A new scheme based on orbital angular momentum in millimetre wave communications for fifth generation," *IET Commun.*, vol. 12, no. 3, pp. 1416–1421, Jul. 2018.
[18] J. Wang, J. Yang, I. M. Fazal, and N. Ahmed, "25.6-bit/s/Hz spectral efficiency using 16-QAM signals over pol-muxed multiple orbital-angular-momentum modes," in *Proc. IEEE Photon. Conf.*, Arlington, VA, USA, Jun. 2011, pp. 587–588.
[19] N. Bozinovic *et al.*, "Terabit-scale orbital angular momentum mode division multiplexing in fibers," *Science*, vol. 340, pp. 1545–1548, Jun. 2013.
[20] F. Tamburini, E. Mari, A. Sponselli, B. Thidé, A. Bianchini, and F. Romanato, "Encoding many channels on the same frequency through radio vorticity: First experimental test," *New J. Phys.*, vol. 14, no. 3, pp. 033001-1–033001-17, Mar. 2012.
[21] W. Cheng, H. Zhang, L. Liang, H. Jing, and Z. Li, "Orbital-angular-momentum embedded massive MIMO: Achieving multiplicative spectrum-efficiency for mmWave communications," *IEEE Access*, vol. 6, pp. 2732–2745, 2017.
[22] J. Lin, X.-C. Yuan, M. Chen, and J. C. Dainty, "Application of orbital angular momentum to simultaneous determination of tilt and lateral displacement of a misaligned laser beam," *J. Opt. Soc. Amer. A, Opt. Image Sci.*, vol. 27, no. 10, pp. 2337–2343, 2010.
[23] A. M. Yao and M. J. Padgett, "Orbital angular momentum: Origins, behavior and applications," *Adv. Opt. Photon.*, vol. 3, no. 3, pp. 161–204, Jun. 2011.
[24] M. Oldoni *et al.*, "Space-division demultiplexing in orbital-angular-momentum-based MIMO radio systems," *IEEE Trans. Antennas Propag.*, vol. 63, no. 10, pp. 4582–4587, Oct. 2015.
[25] Y. Ren *et al.*, "Line-of-sight millimeter-wave communications using orbital angular momentum multiplexing combined with conventional spatial multiplexing," *IEEE Trans. Wireless Commun.*, vol. 16, no. 5, pp. 3151–3161, May 2017.
[26] X. Ge, R. Zi, X. Xiong, Q. Li, and L. Wang, "Millimeter wave communications with OAM-SM scheme for future mobile networks," *IEEE J. Sel. Areas Commun.*, vol. 35, no. 9, pp. 2163–2177, Sep. 2017.
[27] Y. Yuan, Z. Zhang, J. Cang, H. Wu, and C. Zhong, "Capacity analysis of UCA-based OAM multiplexing communication system," in *Proc. Int. Conf. Wireless Commun. Signal Process.*, Oct. 2015, pp. 1–5.
[28] H. Chen, W. Lou, Z. Wang, and F. Xia, "'On achieving asynchronous energy-efficient neighbor discovery for mobile sensor networks," *IEEE Trans. Emerg. Topics Comput.*, to be published, doi: 10.1109/TETC.2016.2586192.
[29] B. Lyu, H. Guo, Z. Yang, and G. Gui, "Throughput maximization for hybrid backscatter assisted cognitive wireless powered radio networks," *IEEE Internet Things*, vol. 5, no. 3, pp. 2015–2024, Jun. 2018.
[30] A. G. Sreedevi and T. R. Rao, "Device-to-device network performance at 28 GHz and 60 GHz using device association vector algorithm," in *Proc. IEEE Int. Conf. Signal Process., Inform., Commun. Energy Syst. (SPICES)*, Aug. 2017, pp. 1–5.
[31] J. Yang, J. J. Werner, and G. A. Dumont, "The multimodulus blind equalization and its generalized algorithms," *IEEE J. Sel. Areas Commun.*, vol. 20, no. 5, pp. 997–1015, Jun. 2002.
[32] I. B. Djordjevic, J. A. Anguita, and B. Vasic, "Error-correction coded orbital-angular-momentum modulation for FSO channels affected by turbulence," *J. Lightw. Technol.*, vol. 30, no. 17, pp. 2846–2852, Sep. 1, 2012.
[33] Z. Zhao, R. Liao, S. D. Lyke, and M. C. Roggemann, "Reed–Solomon coding for free-space optical communications through turbulent atmosphere," in *Proc. IEEE Aerosp. Conf.*, BigSky, MT, USA, Mar. 2010, pp. 1–12.

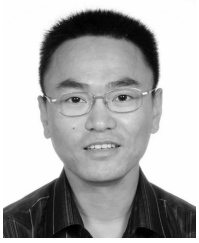

LEI WANG (M'10) received the M.Sc. degree and the Ph.D. degree in telecommunications and information engineering from the Nanjing University of Posts and Telecommunications, China, in 2007 and 2010, respectively. From 2012 to 2013, he was a Post-Doctoral Research Fellow with the Department of Electrical Engineering, Columbia University, USA. He is currently an Associate Professor with the College of Telecommunications and Information Engineering, Nanjing University of Posts and Telecommunications. His research interests include millimeter-wave wireless communications, device-to-device communications, physical-layer security, signal processing for communications, cognitive wireless networks, and random matrix theory.

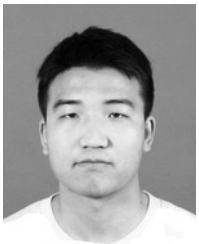

FA JIANG is currently pursuing the M.Sc. degree with the Nanjing University of Posts and Telecommunications, China. His research interests include millimeter-wave wireless communications and device-to-device communications.

MINGKAI CHEN received the M.Sc. degree, with major on communication and information system, from Fuzhou University, China, in 2014. He is currently pursuing the Ph.D. degree with the Nanjing University of Posts and Telecommunications, China. His research interests include wireless multimedia communication and resource allocation in wireless networks.

HAIE DOU received the M.A. degree from Southeast University, China, in 2010. She is currently with the College of Media and Art, Nanjing University of Posts and Telecommunications. Her research interests mainly include art design, computer graphics, image communication, and multimedia information processing.

GUAN GUI (M'11–SM'17) received the Dr. Eng degree in information and communication engineering from the University of Electronic Science and Technology of China, Chengdu, China, in 2012. From 2009 to 2012, with the financial support from the China Scholarship Council and the Global Center of Education, Tohoku University, he was a Research Assistant and a Post-Doctoral Research Fellow, respectively, with the Wireless Signal Processing and Network Laboratory, Department of Communications Engineering, Graduate School of Engineering, Tohoku University, where he was also a Post-Doctoral Research Fellow from 2012 to 2014, with the support from the Japan Society for the Promotion of Science Fellowship. From 2014 to 2015, he was an Assistant Professor with the Department of Electronics and Information System, Akita Prefectural University. Since 2015, he has been a Professor with the Nanjing University of Posts and Telecommunications, Nanjing, China.

He is currently engaged in the research of deep learning, compressive sensing, and advanced wireless techniques. He was selected as the Jiangsu Specially Appointed Professor and the Jiangsu High-Level Innovation and Entrepreneurial Talent, and he was selected for the Nanjing Youth Award. He received several best paper awards in international conferences, such as from CSPS 2018, ICNC 2018, ICC 2017, ICC 2014, and VTC 2014-Spring. He was an Editor of the *Security and Communication Networks* from 2012 to 2016. He has been an Editor of the IEEE TRANSACTIONS ON VEHICULAR TECHNOLOGY and the *KSII Transactions on Internet and Information System* since 2017.

HIKMET SARI (F'95) received the degree in engineering and the Ph.D. degree from the ENST, Paris, France, and the Post-Doctoral Habilitation degree from the University of Paris-Sud, Orsay. He held various research and management positions in industry, including Philips Research Laboratories, SAT, Alcatel, Pacific Broadband Communications, and Juniper Networks. He is currently a Professor with the Nanjing University of Posts and Telecommunications and also a Chief Scientist with Sequans Communications. His distinctions include the André Blondel Medal in 1995, the Edwin H. Armstrong Achievement Award in 2003, and the Harold Sobol Award in 2012, as well as elected to Academia Europaea (the Academy of Europe) and to the Science Academy of Turkey in 2012. He served as an Editor for the IEEE TRANSACTIONS ON COMMUNICATIONS from 1987 to 1991, a Guest Editor for the *European Transactions on Telecommunications* in 1993 and for the IEEE JSAC in 1999, and an Associate Editor for the IEEE COMMUNICATIONS LETTERS from 1999 to 2002. He served as a Distinguished Lecturer for the IEEE Communications Society from 2001 to 2006, and as a member for the IEEE Fellow Evaluation Committee from 2002 to 2007 and the Awards Committee from 2005 to 2007.

Dr. Sari was the Chair of the Communication Theory Symposium of the ICC 2002, New York, the Technical Program Chair of the ICC 2004, Paris, the Vice General Chair of the ICC 2006, Istanbul, the General Chair of the PIMRC 2010, Istanbul, the General Chair of the WCNC 2012, Paris, the Executive Chair of the WCNC 2014, Istanbul, the General Chair of the ICUWB 2014, Paris, the General Co-Chair of the IEEE BlackSeaCom 2015, Constanta, Romania, the Technical Program Chair of the EuCNC 2015, Paris, and the Executive Co-Chair of the ICC 2016, Kuala Lumpur. He also chaired the Globecom and ICC Technical Content Committee during 2010–2011. He was the Vice President of the conferences of the IEEE Communications Society during 2014–2015. He is currently serving as the General Co-Chair for the ATC 2016, Hanoi, Vietnam, the Executive Chair for the ICC 2017, Paris, and the General Chair for the PIMRC 2019, Istanbul.